siRNA screening reveals JNK2 as an evolutionary conserved regulator of triglyceride homeostasis[S]

Vinciane Grimard,* Julia Massier,* Doris Richter,* Dominik Schwudke,* Yannis Kalaidzidis,* Eugenio Fava,* Albin Hermetter,† and Christoph Thiele[1,*]

Max-Planck-Institute of Molecular Cell Biology and Genetics,* Pfotenhauerstrasse 108, 01307 Dresden, Germany; and Institute of Biochemistry,† Graz University of Technology, Petersgasse 12/II, A-8010 Graz, Austria

Abstract Lipid homeostasis is essential for proper function of cells and organisms. To unravel new regulators of this system, we developed a screening procedure, combining RNA interference in HeLa cells and TLC, which enabled us to monitor modifications of lipid composition resulting from short, interfering RNA knock-downs. We applied this technique to the analysis of 600 human kinases. Despite the occurrence of off-target effects, we identified JNK2 as a new player in triglyceride (TG) homeostasis and lipid droplet metabolism and, more specifically, in the regulation of lipolysis. Similar control of the level of TGs and lipid droplets was observed for its *Schizosaccharomyces pombe* homolog, Sty1, suggesting an evolutionary conserved function of mitogen-activated protein kinases in the regulation of lipid storage in eukaryotic cells.—Grimard, V., J. Massier, D. Richter, D. Schwudke, Y. Kalaidzidis, E. Fava, A. Hermetter, and C. Thiele. **siRNA screening reveals JNK2 as an evolutionary conserved regulator of triglyceride homeostasis. *J. Lipid Res.* 2008.** 49: **2427–2440.**

Supplementary key words c-jun N-terminal kinase • HeLa cells • kinase • lipid droplet • mitogen-activated protein kinase-9

Over the past decades, pathologies such as obesity and atherosclerosis have become major health concerns in Westernized societies (1). These pathologies often result from dysregulation of lipid intake and metabolism resulting from the overly rich diet that has become standard in our societies and, increasingly, in developing countries (2).

Considering the wide variety of lipids and the dynamics of their metabolism, it is clear that tight regulatory systems are necessary to maintain lipid homeostasis. Several such systems have already been unraveled. Among them is the sterol-regulatory element binding protein pathway, which is responsible for sensing cholesterol levels and for regulation of cholesterol and fatty acid biosynthesis (3). Several nuclear hormone receptors have also been linked to lipid regulation, in particular, the members of the peroxisome proliferator-activated receptor and liver X receptor subfamilies (4–7). These proteins are transcription factors that are activated upon interaction with small lipophilic molecules such as fatty acids and oxysterols, respectively (8). More recently, several micro-RNAs, small regulatory RNA molecules, have been linked to lipid homeostasis, both in *Drosophila* and in mice (9–12).

However, considering the complexity of the system, it is highly expected that other proteins involved in the regulation of lipid homeostasis still need to be found. The discovery of RNA interference (RNAi) as a tool to specifically decrease the expression level of any gene (13, 14) has opened up new possibilities for large-scale analysis of gene function (15, 16). Kinases have already been implicated in the regulation of numerous cellular processes but are still under-represented in the field of lipid metabolism. Therefore, we set up a screening procedure, combining RNAi and lipid analysis using TLC, to monitor changes in lipid metabolism upon specific gene knock-down induced by short interfering RNA (siRNA). This method was then used to study 600 kinases, and the best candidates were further characterized, giving rise to the identification of c-jun N-terminal kinase 2 (JNK2) as a new regulator of triglyceride (TG) metabolism. Further studies of the homolog of JNK2 in *Schizosaccharomyces pombe*, Sty1, revealed that this process is evolutionary conserved in eukaryotic cells.

C.T. and V.G. were supported by the German Research Foundation (Transregio TR13/D2) and J.M. was supported by the Boehringer Ingelheim Foundation.

Manuscript received 3 April 2008 and in revised form 5 June 2008 and in re-revised form 2 July 2008.

Published, JLR Papers in Press, July 7, 2008.
DOI 10.1194/jlr.M800168-JLR200

Abbreviations: ACAT, acyl-CoA:cholesterol acyltransferase; CE, cholesteryl ester; JNK, c-jun N-terminal kinase; MAPK, mitogen-activated protein kinase; RNAi, RNA interference; siRNA, short, interfering RNA; TG, triglyceride.

[1] To whom correspondence should be addressed.
e-mail: thiele@mpi-cbg.de

[S] The online version of this article (available at http://www.jlr.org) contains supplementary data in the form of two figures and two tables.

TABLE 1. List of siRNAs (Except the Kinase Library)

Gene	ID number	Company	RefSeq Number	Other Names Used in the Thesis or Sequences
ACAT1	4490	Ambion	NM_003101	siRNA1
ACAT1	4586	Ambion	NM_003101	siRNA2
ACAT1	4679	Ambion	NM_003101	siRNA3
CSF1R	641	Ambion	NM_005211	siRNA1 (screen), O1
CSF1R	642	Ambion	NM_005211	siRNA2 (screen), O2
CSF1R	643	Ambion	NM_005211	siRNA3 (screen), O3
CSF1R	146601	Ambion	NM_005211	siRNA1 (new), N1
CSF1R	146602	Ambion	NM_005211	siRNA2 (new), N2
CSF1R	146603	Ambion	NM_005211	siRNA3 (new), N3
EG5	Custom	Ambion	NM_004523	CUGAAGACCUGAAGACAAUtt AUUGUCUUCAGGUCUUCAGtt
IKK1 (CHUK)	112	Ambion	NM_001278	siRNA1 (screen), O1
IKK1 (CHUK)	113	Ambion	NM_001278	siRNA2 (screen), O2
IKK1 (CHUK)	114	Ambion	NM_001278	siRNA3 (screen), O3
IKK1 (CHUK)	145720	Ambion	NM_001278	siRNA1 (new), N1
IKK1 (CHUK)	145721	Ambion	NM_001278	siRNA2 (new), N2
IKK1 (CHUK)	145722	Ambion	NM_001278	siRNA3 (new), N3
JNK2	1452	Ambion	NM_002752	siRNA1 (screen), O1
JNK2	1547	Ambion	NM_002752	siRNA2 (screen), O2
JNK2	1637	Ambion	NM_002752	siRNA3 (screen), O3
JNK2	142316	Ambion	NM_002752	siRNA1 (new), N1
JNK2	142317	Ambion	NM_002752	siRNA2 (new), N2
JNK2	142318	Ambion	NM_002752	siRNA3 (new), N3
JNK2	SI00300797	Qiagen	NM_002752	
RIPK4	1177	Ambion	NM_020639	siRNA1 (screen), O1
RIPK4	1272	Ambion	NM_020639	siRNA2 (screen), O2
RIPK4	1367	Ambion	NM_020639	siRNA3 (screen), O3
RIPK4	113612	Ambion	NM_020639	siRNA1 (new), N1
RIPK4	113613	Ambion	NM_020639	siRNA2 (new), N2
RIPK4	133160	Ambion	NM_020639	siRNA3 (new), N3
S2	AM4613	Ambion		Silencer negative control #2
S5	AM4642	Ambion		Silencer negative control #5
S6	AM4643	Ambion		Silencer negative control #6
TRIO	848	Ambion	NM_007118	siRNA1 (screen), O1
TRIO	849	Ambion	NM_007118	siRNA2 (screen), O2
TRIO	103343	Ambion	NM_007118	siRNA3 (screen), O3
TRIO	103427	Ambion	NM_007118	siRNA1 (new), N1

siRNA, short, interfering RNA.

MATERIALS AND METHODS

Materials

High-glucose DMEM, Opti-MEM, FBS, and trypsin were obtained from Gibco (Karlsruhe, Germany). Delipidated FBS was prepared as described previously (17). Oleate was from Acros (Geel, Belgium). [^{14}C]acetate was obtained from Amersham (Freiburg, Germany) and [^{3}H]oleate from Hartmann Analytic (Braunschweig, Germany).

The siRNA kinase library was obtained from Ambion (Austin, TX). Other siRNAs were also from Ambion, unless otherwise indicated, and are described in **Table 1**.

Real-time PCR primers were from Biospring (Frankfurt, Germany). Sequences can be found in **Table 2**. Rabbit polyclonal antibody against IKK1 was from Santa Cruz (Heidelberg, Germany). HRP-conjugated donkey anti-rabbit IgG secondary antibody was from Jackson Immunological (West Grove, PA).

Sty1 deletion strain of *S. pombe* (JM1160, L972 h$^-$ sty1::ura4 leu1-32 ura4-D18 ade6) and its parent wild-type strain (PR109, L972 h$^-$ leu1-32 ura4-D18) were a kind gift from Dr. J. B. Millar (University of Warwick, UK).

Cell culture

HeLa cells and A431 cells were cultured in DMEM supplemented with 10% FBS. Cells were passaged regularly using trypsin to maintain them in exponential growth phase and were tested for the absence of mycoplasma on a regular basis.

TABLE 2. List of RT-PCR Primers

Gene	Forward Primer	Reverse Primer
ACAT1	CACGTTCCTGGACTTGTCGTTAC	TCAGGGAGCTACCCAATCTTCA
GAPDH-1	TCGACAGTCAGCCGCATCT	CCCCATGGTGTCTGAGCG
GAPDH-2	CAAGGTCATCCATGACAACTTTG	GGCCATCCACAGTCTTCTGG
Tubulin	ACTGGCATCCTGCTTTCCAGT	GGCTCTGTAGCTCCCCATGTACT
IKK1	CAAGATGGGGAGACTTCAGC	ATTGCCCTGTTCCTCATTTG
TRIO	AAGCAGCAGCAGTAGCAACA	TTTGAACGACCTCTCCTTGG
RIPK4	AGGATGAGGACCAGTGGACA	GAGGCGTTCTTCTCCAACAG
JNK2	CTGCGTCACCCATACATCAC	CTTTCTTCCAACTGGGCATC

siRNA transfection

Four thousand HeLa cells were plated in 80 μl growth medium in each well of a 96-well plate 20 h before transfection. Oligofectamine (Invitrogen, Karlsruhe, Germany) was mixed with Opti-MEM medium in a 1:6.5 ratio and incubated for 5 min. For each well, a mix of 10 pmol siRNA in 17 μl Opti-MEM medium and 3 μl of the oligofectamine mix was prepared. This was incubated for 20 min to allow formation of the cationic liposome-RNA complex and then added to the cells. For the screen, the transfection procedure was automated and performed on a Tecan Freedom Evo workstation (Tecan, Mannedorf, Switzerland) under sterile conditions. Growth medium was exchanged 48 h after transfection for 100 μl DMEM medium supplemented with 10% delipidated FBS. For lipid analysis by TLC, 2 μCi [^{14}C] acetate was added in each well 56 h after transfection. Lipid extracts or cells were harvested 72 h after transfection.

One-phase lipid extraction and TLC analysis

Lipids were extracted directly from the wells of a 96-well plate using 15 μl MeOH-$CHCl_3$ (5:1) and applied onto silica 60 TLC plates (Merck, Darmstadt, Germany). The plates were developed in a glass chamber containing EtOH-water-triethylamine-$CHCl_3$ (5:1:3.5:3.5) up to two-thirds of the plate, dried, and then further developed with hexane-ethylacetate (5:1) up to the top of the plate (18). TLC plates with radioactive samples were exposed on a phosphorimager plate for 1 to 3 days and subsequently read using a phosphorimager BAS1800II (Fuji, Dusseldorf, Germany).

Lipid profile comparison and quantification

For analysis of the TLC plates, the radioactive signal obtained with the phosphorimager was initially analyzed using Image Gauge (Fuji). Individual lipid intensity profiles were recovered via this software and then transferred to Graph Explorer (19). For profile comparison, lipid intensities were normalized to the level of phosphatidylcholine (PC). The choice of PC rather than total radioactive counts was necessary to avoid the contribution of free radioactive acetate, which may vary from one sample to another. Because PC is the most abundant peak and did not seem to vary among the samples, we opted for this peak for normalization. When necessary, alignment of the profiles was also performed. For quantification of the TG and cholesteryl ester (CE) levels in acyl-CoA:cholesterol acyltransferase 1 (ACAT1) knock-down, the peaks corresponding to TG and CE were fitted using Gaussian curves. The area below the different curves was retrieved, and the TG/CE ratio was normalized to the ratio of the nontransfected negative control.

Clustering

The different phenotypes were first converted into a numerical representation. For each lipid peak, a phenotype readily visible on the TLC plate was assigned a value of 3, and a phenotype revealed by profile comparison was assigned a value of 2. The numerical table was loaded into CUPID (Scionix, Dresden, Germany) and clustered by k-means clustering using Pearson correlation. Annotation was performed using CUPID and corrected manually when needed.

Treatment with parthenolide

For inhibition of IKK, parthenolide (Biomol International, Exeter, UK) was added to the cells at the indicated concentrations, followed by the addition of 2 μCi [^{14}C]acetate after 6 h. Lipid extraction and TLC analysis were performed after 24 h.

Treatment with SP600125

For inhibition of JNK2, SP600125 (Sigma, St. Louis, MO) was added to the cells at a final concentration of 5 μM, followed by the addition of 2 μCi [^{14}C]acetate after 6 h. Lipid extraction and TLC analysis were performed after 24 h.

Oleate feeding

Oleate was added to the cells 4 h after transfection, to a final concentration of 50 μM. In addition, 1 μCi of [^{3}H]oleate was added as a tracer in each sample. Lipids were extracted as described above 48 h after transfection and separated by TLC. The TLC plate was then dipped in LumaSafe solution (Lumac LSC, Groningen, The Netherlands) and exposed on MP films (Amersham) for 6 h at −80°C.

NBD-HEP treatment

siRNA-transfected cells were treated with 1 nmol/well (10 μM) of NBD-D-HP 48 h after transfection. [^{14}C]acetate (2 μCi) was added in each well 56 h after transfection. Lipids were extracted 72 h after transfection and separated by TLC as described above.

MS

Lipid extracts were obtained 72 h after siRNA transfection. Lipids were extracted using 100 μl MeOH-$CHCl_3$ (5:1). The extract was transferred to a 1.5 ml Eppendorf tube (Eppendorf, Hamburg, Germany). Chloroform (100 μl) and 100 μl H_2O were added, and tubes were thoroughly vortexed, then centrifuged at 1,000 *g*. The organic phase was transferred into a new tube and dried down in a SpeedVac. Samples were then resuspended in 100 μl MeOH-$CHCl_3$-isopropanol (2:1:4) supplemented with 7.5 mM ammonium acetate. MS analysis was performed on a LTQ Orbitrap (ThermoElectron, San Jose, CA) equipped with a NanoMate HD robotic nanoflow ion source (Advion BioSciences, Ithaca, NY) with a 4.1 μm nozzle diameter chip. NanoMate HD was operated in positive-ion mode at an ionization voltage of 1.05 kV and gas pressure of 1 psi. A list of peaks was then retrieved using Qualbroser 2.0 (Thermo Fischer Scientific, Bremen, Germany). The average intensity of every sample was calculated using the intensity of the most abundant lipid species, PC 34:1, and used for normalization.

RNA extraction and real-time PCR

RNA was isolated using the RNeasy kit (Qiagen, Hilden, Germany) according to the manufacturer's protocol. For each sample, the contents of three wells were pooled. To remove DNA contamination, 10 units RNase-free DNase I (Boehringer Ingelheim, Ingelheim, Germany) was added to each sample in a 10× DNase buffer (0.4 M Tris, 0.1 M NaCl, 60 mM $MgCl_2$ in RNase-free water, pH 7.5) and incubated for 30 min at 37°C, followed by 20 min at 65°C, cooled on ice and spun down. RNA was heated to 70°C for 10 min to destroy secondary structures, cooled on ice, and spun down. Reverse transcription was carried out according to the manufacturer's protocol (Promega, Mannheim, Germany). For real-time PCR, cDNA was mixed with a 2× SYBR green mix (ABgene, Hamburg, Germany) and forward and reverse primer mix (250 nM final each) to a final volume of 10 μl. Primers are listed in Table 2. Real-time PCR was carried out on an Mx3000 instrument (Stratagene, Amsterdam, The Netherlands). The housekeeping genes tubulin or GAPDH were used for normalization.

SDS-PAGE and Western blotting

Lysates were obtained by the direct addition of Laemmli sample buffer onto the cells. After heating and sonication, proteins

were separated by SDS-PAGE and transferred onto nitrocellulose using a semi-dry blot system (Bio-Rad, Munich, Germany). Blocking was performed overnight at 4°C in PBS supplemented with 0.2% Tween 20 and 5% milk. Incubations with both primary and secondary antibodies were performed at room temperature for 1 h in the same solution as for the blocking. After each antibody incubation, blots were extensively washed in PBS supplemented with 0.2% Tween 20. Signal was detected using ECL (Amersham).

BODIPY 493/503 staining and microscopy

Four thousand A431 cells were plated in 400 μl growth medium in each well of a 24-well plate 20 h before transfection. For each well, 14 pmol siRNA was mixed with 100 μl Opti-MEM medium and 6 μl Hiperfect (Qiagen, Hilden, Germany). The siRNA mix was incubated for 10 min to allow formation of the cationic liposome-RNA complex and then added to the cells. Forty-eight hours after transfection, growth medium supplemented with 20 μM oleate or with DMEM supplemented with 10% delipidated FBS was exchanged for the growth medium. Seventy-two hours after transfection, cells were washed once with PBS and fixed with 5% formaldehyde in PBS for 1 h at room temperature. Cells were washed once again with PBS, and BODIPY 493/503 (MoBiTec, Götingen, Germany) was added to the cells at a final concentration of 2 μg/ml. Staining was performed in the dark for 1 h at room temperature. After extensive washes with PBS, cells were mounted on slides using 6 μl Mowiol (CalBiochem, La Jolla, CA). Images were acquired on a Zeiss Axiovert 200 inverted confocal microscope (Jena, Germany) equipped with a 63× Plan-Apochrom oil objective.

S. pombe culture

S. pombe cultures were grown in Edinburgh minimal medium supplemented with 225 mg/l uracil, adenine, and L-leucine (Sigma) (20), either on an agar plate at 30°C or in liquid cultures in a shaking incubator at 30°C and 200 rpm.

Nile Red staining and microscopy

S. pombe pellets were obtained by centrifugation of 2 ml culture, resuspended in 0.5 ml PBS supplemented with 3 μg Nile Red (Sigma) and incubated for 10 min in the dark at room temperature and 1,000 rpm. Cells were washed twice with PBS and resuspended in 200 μl PBS. Two microliters were used for microscopy. Images were acquired on an Olympus AX70 upright microscope (Hamburg, Germany) equipped with a 100× UplanApo oil objective and a CCD camera controlled by Metavue software (Universal Imaging Corporation, Downingtown, PA).

S. pombe lipid extraction and TLC

[^{3}H]oleate (1 μCi/ml) was added to the yeast culture 3 h before lipid extraction. *S. pombe* pellets were obtained by centrifugation of 5 ml culture and washed twice with H_2O. The pellets were then resuspended in 1 ml MeOH-$CHCl_3$ (2:1). Samples were homogenized using vigorous beating in the presence of glass beads (Sigma) for 2 min. After centrifugation, supernatants were transferred into new tubes with 400 μl of 50 mM citric acid and 600 μl $CHCl_3$. The organic phase was transferred to a new tube and evaporated under a nitrogen stream. Lipids were then resuspended in 30 μl MeOH-$CHCl_3$ (2:1) and were separated by TLC as described above. The TLC plate was then dipped in LumaSafe solution (Lumac LSC) and exposed on MP films (Amersham) for 16 h at −80°C.

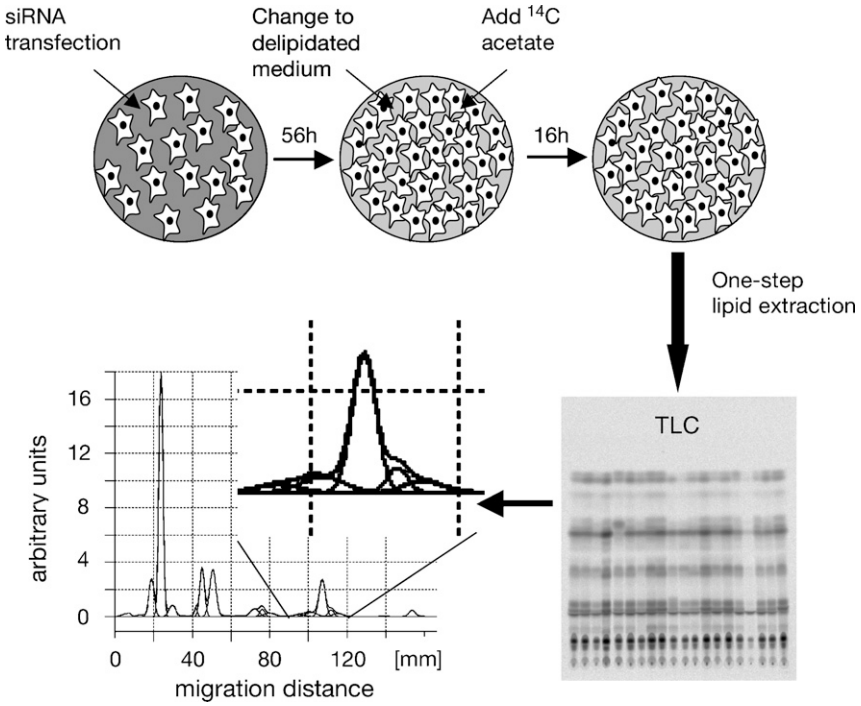

Fig. 1. Schematic representation of the method. HeLa cells were transfected with short interfering RNA (siRNA) against controls and various kinases. After 56 h, medium was exchanged for a delipidated medium and radioactive acetate was added. After another 16 h, lipids were extracted and separated by TLC, followed by identification and quantification of radioactive lipid classes.

RESULTS

A screen to unravel lipid homeostasis

The absence or mutation of a gene implicated in lipid homeostasis affects the lipid composition of a cell. Therefore, we designed a method to monitor these changes by combining RNAi with TLC analysis of lipid extracts obtained 3 days after transfection of HeLa cells. To visualize lipids, cells were fed 16 h before extraction with radioactive acetate, the building block of all major lipids. Consequently, its incorporation allowed the radioactive detection of the newly synthesized lipids. Furthermore, to promote lipid synthesis and increase the signal, cells were transferred to a growth medium containing serum devoid of lipids. A schematic representation of the method can be found in **Fig. 1**.

Appropriate controls are essential in the design of large-scale experiments. As negative controls, we used mock transfection as well as transfection with an siRNA targeting the neomycin resistance gene, or scrambled siRNAs (S2, S5, and S6), which do not target any gene in the genome. ACAT1 was selected as a positive control. This enzyme is responsible for the esterification of cholesterol. We tested the efficiency of three independent siRNAs targeting ACAT1 by monitoring the decrease in mRNA level after RNAi by real-time PCR (see supplementary Fig. IA). Two of the three siRNAs tested, as well as a pool of the three sequences, induced a decrease of the mRNA level by more than 80%. Using TLC, we observed a strong decrease in the CE level for the same sequences (see supplementary Fig. IB, C), confirming that ACAT1 could be used as a positive control for this screen. In addition, to measure transfection efficiency, the previously characterized eg5 gene was selected (21, 22). This gene encodes for a kinesin-related protein implicated in mitosis. Upon knock-down, cells arrest in mitosis and ultimately die. This results in the absence of a radioactive signal on the TLC plate. We also confirmed, by both TLC and MS, that no significant variation in lipid composition was induced by the lipophilic transfection reagent alone (data not shown).

The screen was performed using an siRNA library, designed by Ambion, which targets 600 kinases, each of them with three siRNA sequences. Individual siRNA sequences vary in efficiency in a manner not yet fully understood (21, 23, 24). To ensure a high efficiency for each kinase, interference was achieved using a pool of the three individual sequences. We hypothesized that at least one of these would be sufficiently potent to reach a good knock-down efficiency, as suggested by the observations made using ACAT1 siRNAs (see supplementary Fig. IA). The screen was carried out in a 96-well plate format, although only the 60 internal wells of the plates were used, to avoid unspecific effects related to medium evaporation in the external wells. Each row contained either a well transfected with the pool of ACAT1 siRNAs, used as a positive control, or a well mock-transfected as a negative control. Because samples from two subsequent rows were applied on one TLC plate, each TLC plate contained at least a positive and a negative control. In addition, several wells

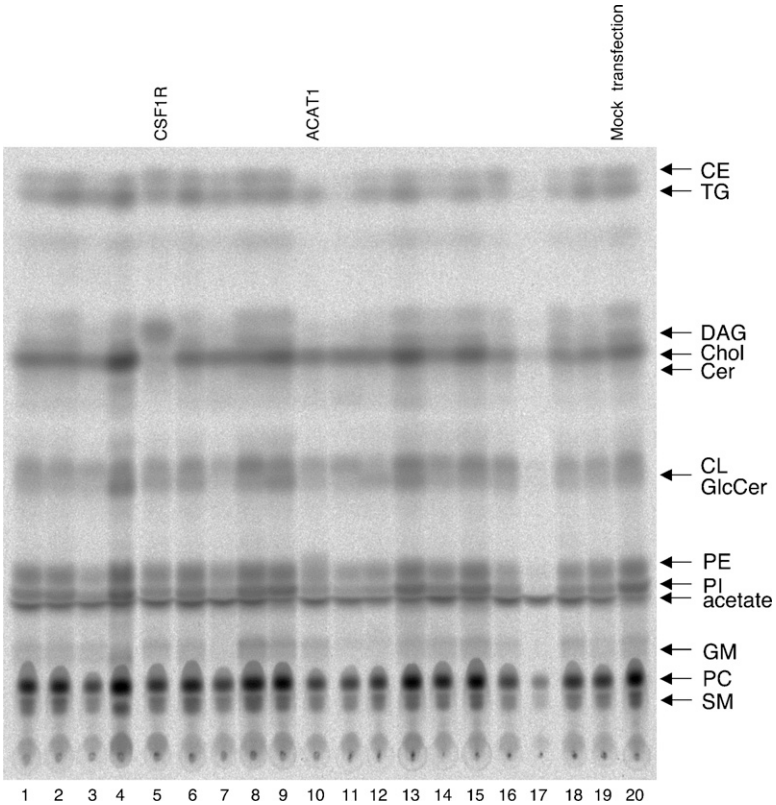

Fig. 2. Typical TLC plate from the screen. After siRNA transfection and [^{14}C]acetate labeling, lipids were separated on a TLC plate. Each vertical lane corresponds to the lipid extract of a kinase or control knock-down. The positions of the different lipid classes are indicated on the right of the plate. ^{14}C-labeled lipids were visualized by exposure to a phosphorimager plate. Samples loaded on this plate were treated with the following siRNAs: *1*), CKB; *2*), CKM; *3*), CKMT1; *4*), CKMT2; *5*), CSF1R; *6*), DCK; *7*), DGKA; *8*), DGKB; *9*), DGKD; *10*), ACAT1; *11*), DGKQ; *12*), DGKZ; *13*), DGUOK; *14*), KFZP586B16; *15*), DTYMK; *16*), EKI1; 17), FLJ10761; *18*), FLJ10842; *19*), FLJ11149; *20*), mock transfection. CE, cholesteryl ester; DAG, diacylglycerol; Chol, cholesterol; Cer, ceramide; CL, cardiolipin; GlcCer, glucosyl ceramide; PE, phosphatidylethanolamine; PI, phosohatidylinositol; GM, ganglioside GM3; PC, phosphatidylcholine; SM, sphingomyelin; TG, triglyceride.

dispersed in the plates were transfected with either the positive control, eg5, or the negative control, S2.

Lipid extracts from the siRNA-transfected cells were then separated by TLC. A sample TLC plate is shown in **Fig. 2**. Each plate contains both the positive control ACAT1 and the negative mock-transfection control (Fig. 2, lanes 10 and 20, respectively). The other samples were derived from the kinase knock-downs or other controls. High reproducibility was observed between the triplicates (see supplementary Fig. II). Out of the 600 kinases, 35 were identified whose knock-down induces a modification of lipid composition readily visible on the TLC plate. The levels of cholesterol or TG were primarily affected in these knock-downs. For further analysis, the radioactive signal from each lane of the TLC was extracted as a lipid intensity profile (Fig. 1, last step). These profiles were normalized to the level of PC and superimposed using the program Graph Explorer (19), in order to compare the intensities of the lipid bands. This analysis extended the number of gene knock-downs inducing a phenotype to 91.

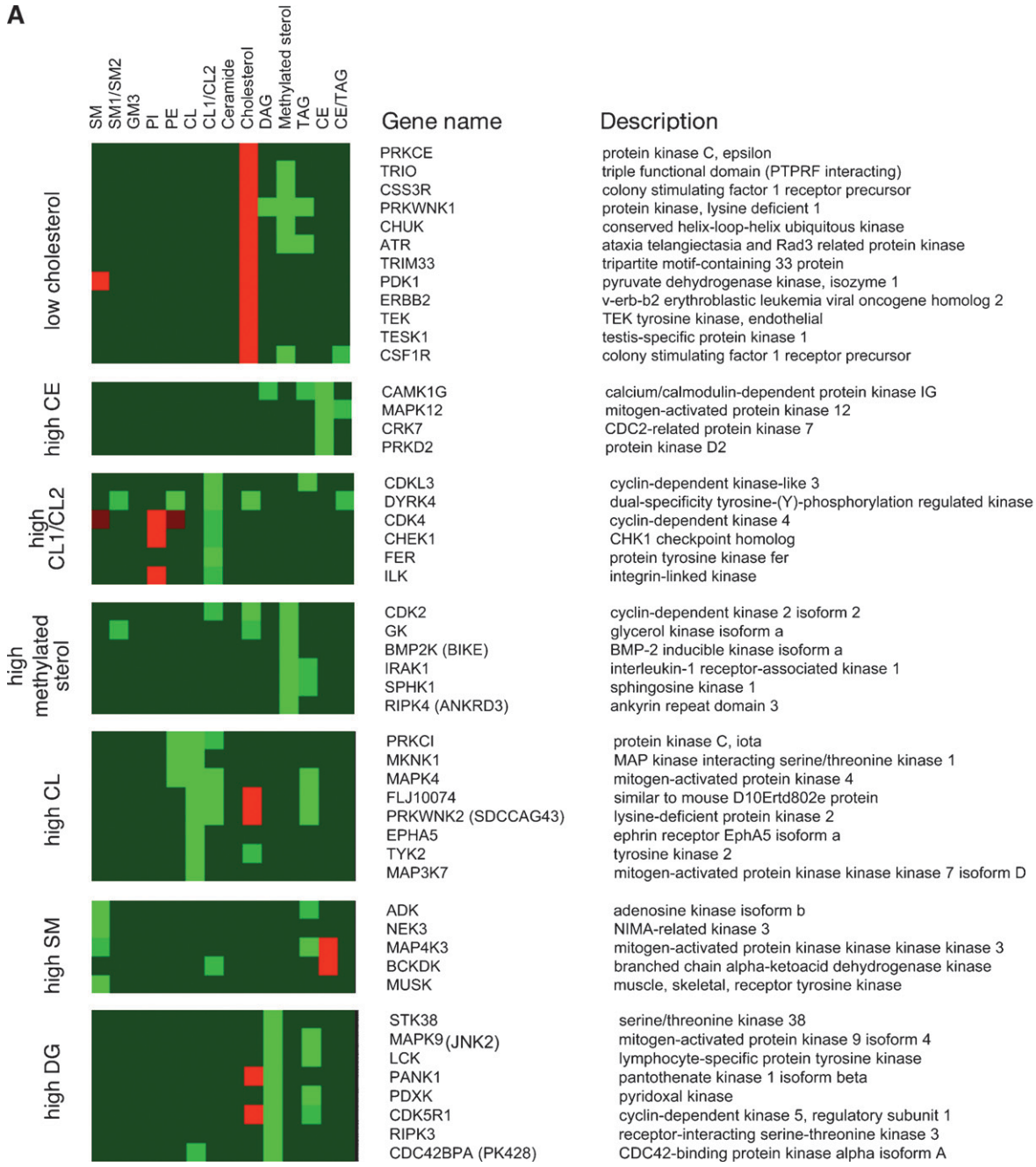

Fig. 3. Clustering of the 91 phenotypic lipid profiles generated by the screen of 600 human kinases. Clustering, which was performed using the program *CUPID* and Pearson correlation, generated 10 phenotypic clusters. Phenotypes were described as increased (green) or decreased (red) in lipid classes or ratios. Annotation was performed using CUPID and corrected manually when needed. TAG, triacylglycerol.

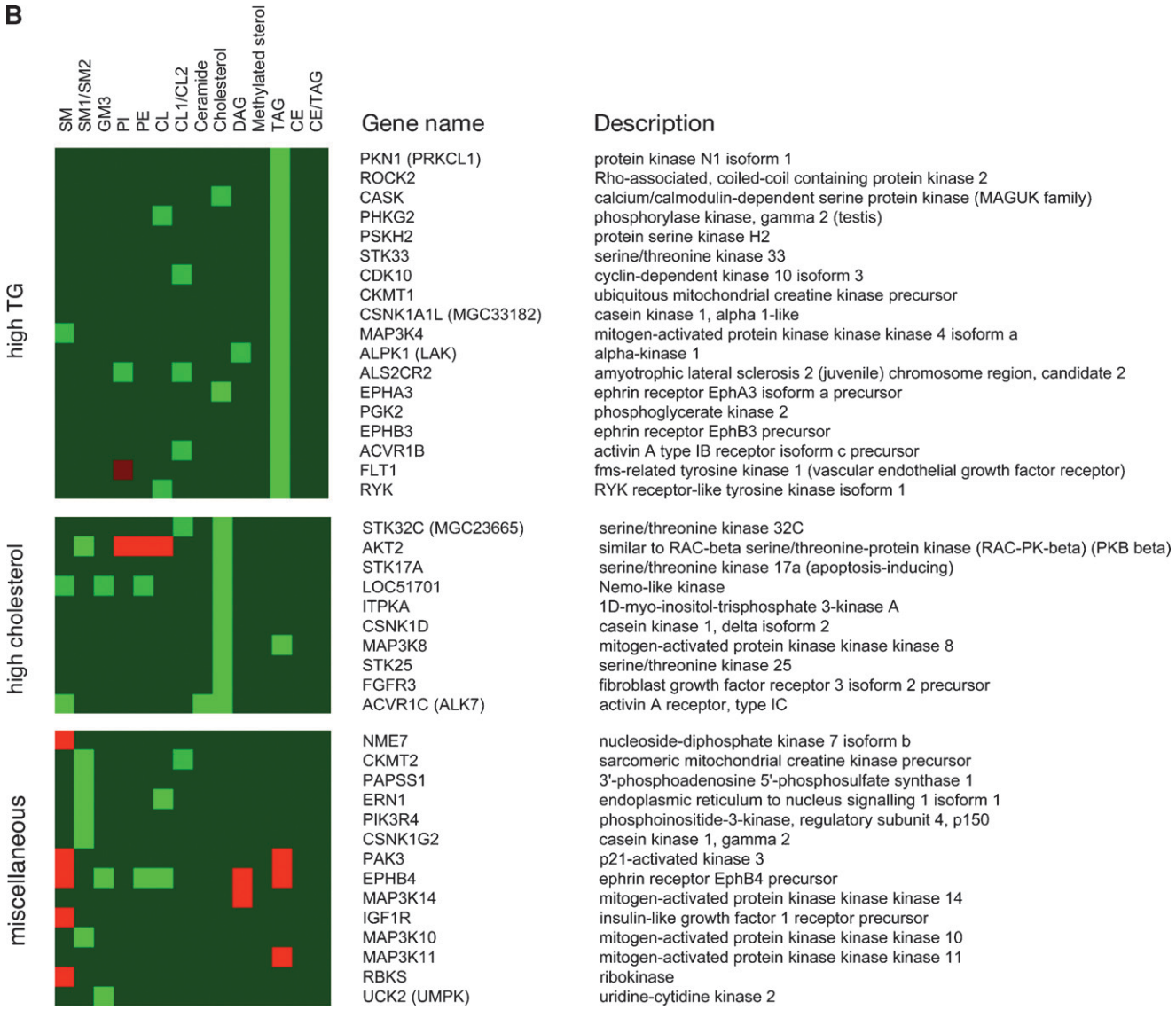

Fig. 3.—*Continued.*

The kinases were then clustered according to lipid profiles of the respective siRNA knock-down (**Fig. 3**), and 10 phenotypic classes characterized by their lipid phenotype were identified. It must be noted that no correlation was observed between the kinase groups generated by the clustering and the kinase subfamilies. This suggests that different members of the same family of kinases are implicated in different biological processes, whereas several kinases from different families can act together or independently in a specific regulation process.

Among the phenotypes observed, several siRNAs induced a decrease in cholesterol and the appearance of an additional lipid band running slightly further than cholesterol (example for CSF1R on Fig. 2, lane 5). This band could be due to the accumulation of an intermediate of cholesterol biosynthesis. The TLC migration of several sterols was then monitored (data not shown). Among the sterols tested, the methylated sterols lanosterol and lophenol showed migratory properties similar to those of the new lipid band. On the basis of the biosynthetic pathway of cholesterol in humans, this new band is likely to be the result of the accumulation of the tri- or dimethylated precursors of cholesterol biosynthesis (lanosterol or demethyllanosterol, respectively).

Off-target effects

Because of the importance of cholesterol in cellular functions, we decided to further analyze the genes showing the strongest cholesterol/methylated sterol phenotype. For the four kinases selected, a new set of three siRNAs of different sequences was used to validate these results (for TRIO, only one new sequence previously characterized was used). However, for all the genes tested, although the phenotype could be reproduced using the pool of sequences used during the screen (**Fig. 4A**, black arrows), there was no new lipid accumulating after treatment with

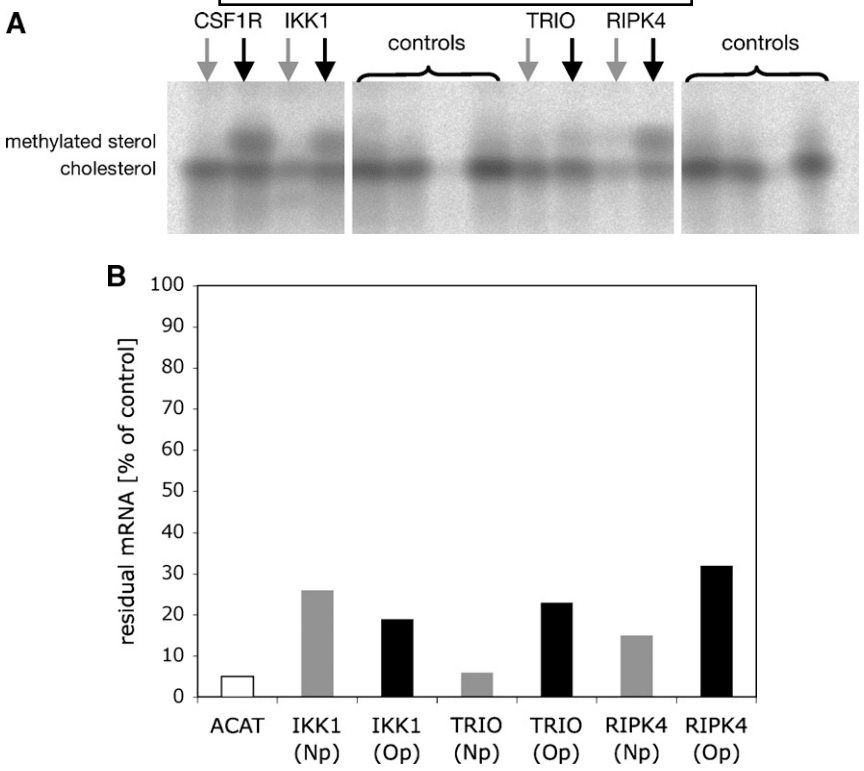

Fig. 4. Lipid phenotype upon siRNA treatment. A: Lipid extracts from HeLa cells treated with pools of three siRNAs from the screen (black arrows, Op), or pools of three siRNAs of new sequences (only one in the case of TRIO) (gray arrows, Np), were separated on TLC plates and compared with controls in the following order: mock transfection, ACAT1, eg5, and no transfection. A close-up of the cholesterol/methylated sterol region of the TLC plate is shown. ^{14}C-labeled lipids were visualized by exposure to a phosphorimager plate. B: RNA was extracted from HeLa cells from the same transfection as above [Op, pools of three siRNAs from the screen; Np, pools of three siRNAs of new sequences (only one in the case of TRIO)]. The mRNA level of the targeted genes was measured by real-time PCR and normalized to GAPDH mRNA. The level of the corresponding mRNA for mock-transfected samples was set to 100%.

the new sequences (Fig. 4A, gray arrows). This strongly suggested that the phenotype observed during the screen was sequence dependent. To check whether the difference in phenotypes could result from the variation in silencing efficiency between the sequences, mRNA levels of the corresponding genes were measured using real-time PCR after siRNA treatment (Fig. 4B). However, for most of the genes tested, the new set of sequences (gray bars) induced a stronger decrease in mRNA level than the sequences used during the screen (black bars). Therefore, the loss of phenotype observed could not result from a decreased silencing efficiency. The phenotype and mRNA level were also analyzed after treatment with individual siRNA sequences. As an example, the lipid phenotypes obtained using siRNAs targeting IKK1 are shown in **Fig. 5A**. Out of the six sequences tested, only two induced the accumulation of the new lipid band, confirming the sequence dependency of the phenotype. The silencing efficiency of these siRNAs was then monitored both at the mRNA level by real-time PCR and at the protein level by Western blots (Fig. 5B, C). At the mRNA level, the best knock-down was observed for the individual sequence O_2, although this sequence did not induce any lipid phenotype. In Western blot, no proteins were detectable after treatment with any of the siRNAs against IKK1, suggesting a strong silencing potency of all the sequences against this protein, even if the silencing at the mRNA level was not complete. This suggests that another silencing mechanism, other than mRNA cleavage, may also take place. Furthermore, this rules out the possibility that the difference in lipid phenotype observed could be due to a variation in protein silencing. Finally, HeLa cells were treated with parthenolide, a known inhibitor of IKK1 (25). Upon increasing the concentration, parthenolide induced cell death, but no accumulation of a new lipid band or decrease in cholesterol (Fig. 5D).

This leads to the conclusion that the lipid phenotype observed was not due to a decrease in the targeted genes, but probably to the decrease of another yet-unidentified gene, a phenomenon known as off-target effect (26).

Analysis of a wider set of genes was then carried out. This set included two kinases whose knock-down induced a strong decrease in one sphingomyelin band, and twelve kinases whose knock-down induced an increase in TG. As for the previous kinases, for all genes tested but one, only one or two siRNA sequences were responsible for the

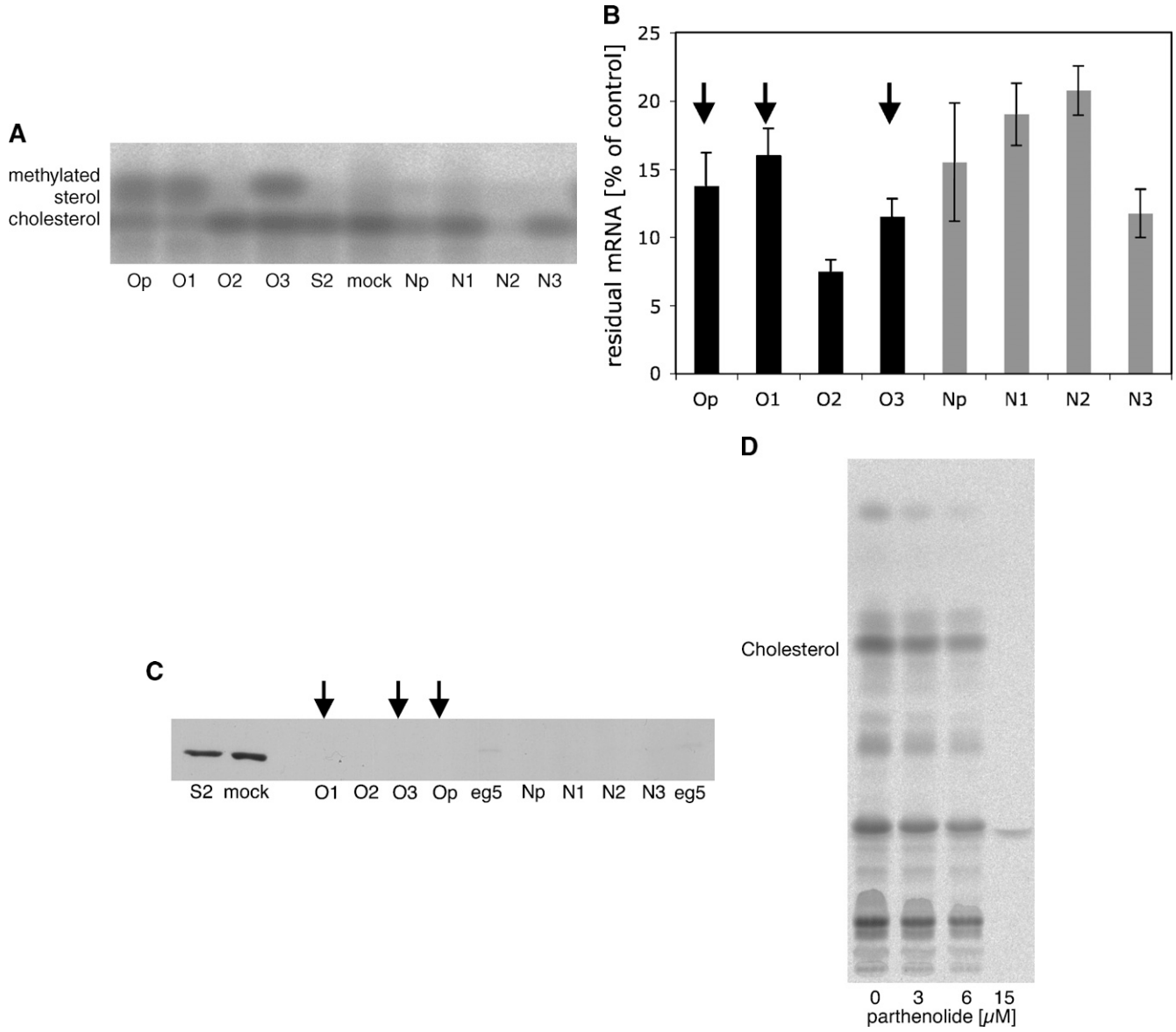

Fig. 5. Analysis of IKK1 knock-down. A: Lipid extracts from HeLa cells treated with a pool of three siRNAs against IKK1 from the screen (lane Op) or the corresponding individual sequences (lanes O1-O3), or with a pool of three siRNAs of new sequences (lane Np) or the corresponding individual sequences (lanes N1–N3), were compared with the S2-treated and mock-transfected control cells. A close-up of the cholesterol/methylated sterol region of the TLC plate is shown. ^{14}C-labeled lipids were visualized by exposure to a phosphorimager plate. IKK1 mRNA levels (B) and protein levels (C) were measured in HeLa cells from the same transfection as above. mRNA levels were measured by real-time PCR and normalized as in Fig. 4. Error bars represent standard deviation (n = 4). C: Protein levels were analyzed by Western blotting with anti-IKK1 and compared with the mock-transfected control and S2-treated cells. The very low level of IKK1 protein in the eg5 controls is due to the fact that most of the cells died in this transfection, indicating good transfection efficiency, and were therefore eliminated through the rinsing steps. B, C: Arrows indicate the samples that gave a lipid phenotype. D: HeLa cells were grown in the presence of various concentrations of the IKK inhibitor parthenolide for 24 h and labeled with [^{14}C]acetate for 18 h. Lipid extracts were separated using TLC. ^{14}C-labeled lipids were visualized by exposure to a phosphorimager plate.

lipid phenotype observed, and, when tested, no correlation could be found between the phenotype observed and the decrease in mRNA level (data not shown).

JNK2 as a modulator of lipid droplet metabolism

Among the siRNAs tested, three out of six sequences directed against the mitogen-activated protein kinase (MAPK) JNK2 induced an increase in TG (**Fig. 6A**) as well as a weak decrease in diacylglycerol (DAG). This result was further confirmed using a fourth sequence from another company (data not shown). Moreover, SP600125, an inhibitor of JNK (27), also induced an increase in TG, further suggesting the specificity of the phenotype (Fig. 6C). As seen in Fig. 6A, one of the siRNA sequences also induced an increase in the level of another storage lipid, CE. To date, we cannot distinguish between an off-target effect of this sequence or a physiological relevance for the concomitant increase of these two classes of storage lipids.

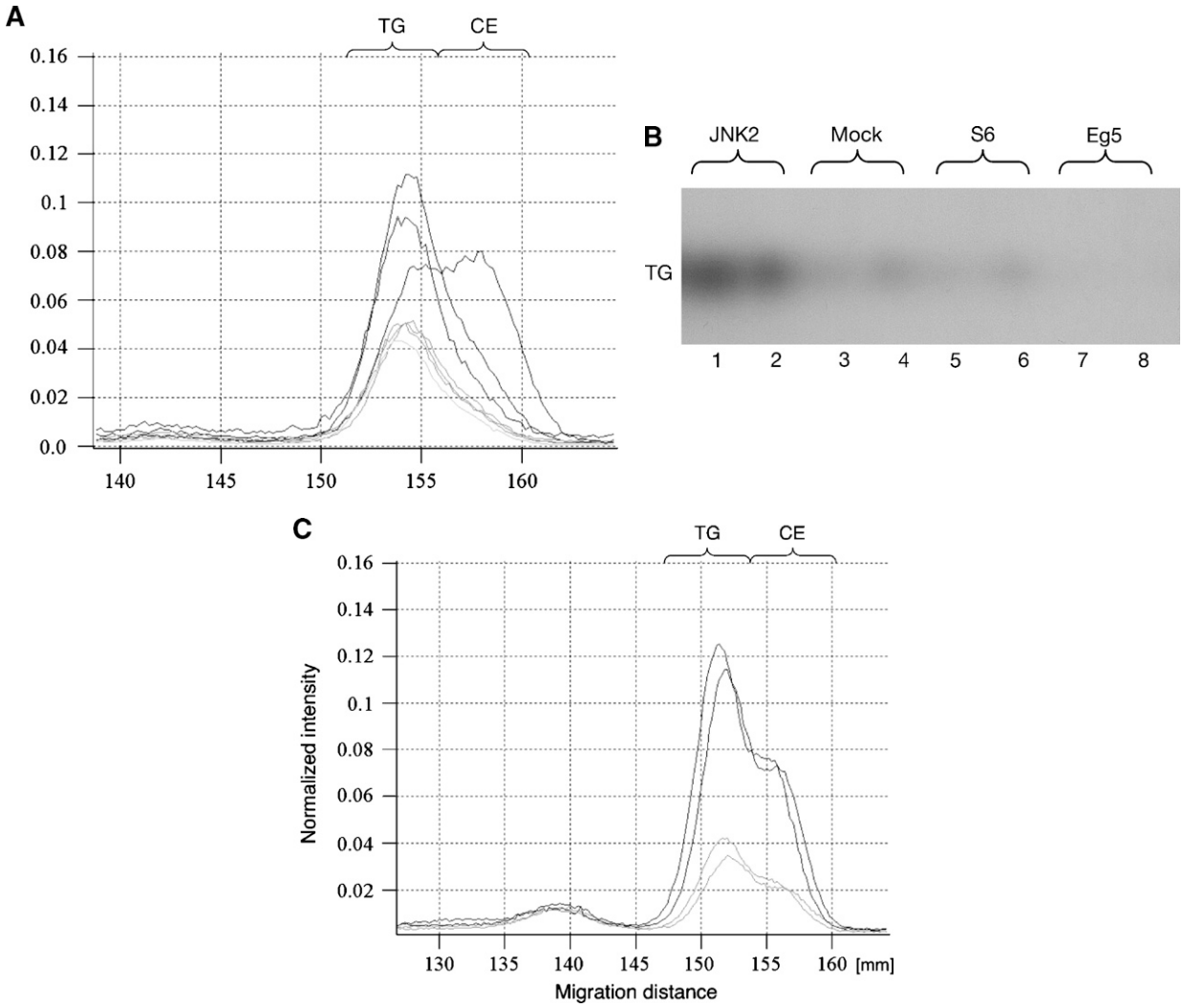

Fig. 6. Increase of TG upon JNK2 knock-down. A: After siRNA transfection and [^{14}C]acetate labeling, lipids were separated on a TLC plate. A close-up of the storage lipid region from the lipid profiles obtained after TLC is shown. Intensities were normalized to the level of PC. The light-gray profile represents the mock-transfected negative control, the dark-gray profiles, the effect of siRNAs O1, N1, and N3 targeting JNK2, showing no phenotype, and the black profiles, the effects of siRNAs O2, O3, and N2 targeting JNK2, showing an increase in TG level. The siRNA N2 shows in addition an increase in the signal corresponding to the upper band, CE, recognizable here by the shoulder in the TG peak. B: HeLa cells were fed with oleate and radioactive oleate 4 h after siRNA transfection. Lipids were extracted 48 h after transfection and separated by TLC. The radioactive signal was revealed by autoradiography. siRNAs used for transfection are indicated on the figure. A pool of the three sequences from the screen (Op) was used for JNK2. A duplicate is shown for each condition. C: HeLa cells were treated with 5 μM SP600125 in DMSO (black curves) or with DMSO alone (grey curves). After ^{14}C labeling, lipids were separated on a TLC plate. A close-up of the storage lipid region from the lipid profiles obtained after TLC is shown. Intensities were normalized to the level of PC.

The phenotype was then further confirmed by independent methods. The increase in TG was monitored upon oleate feeding and radioactive oleate labeling for the JNK2 knock-down versus the controls (Fig. 6B). This experiment confirms that the phenotype is independent of the lipid availability of the cells, because the increase in TG is visible both in lipid-free conditions, i.e., during the screen, and in lipid-rich conditions, as shown in Fig. 6B. Intracellular TG is found in specific organelles called lipid droplets (28). These organelles can be specifically labeled using the lipid droplet dye BODIPY 493/503 (29). Upon JNK2 knock-down, we observed an increase in BODIPY 493/503 staining in lipid-free conditions (**Fig. 7**, upper row), whereas almost no lipid droplets were present in wild-type cells under these conditions. Although weaker, this effect was also observed in lipid-rich, i.e., oleate-fed, cells (Fig. 7, lower row).

Finally, we used lipid MS to monitor the phenotype. MS using the LTQ Orbitrap allowed, on the basis of accurate mass measurements, the monitoring of 90 lipid species, or at least the sum of the isobaric species (30), distributed in seven lipid classes (data not shown). Only the relative abundance of TG species was significantly perturbed upon treatment with siRNA against JNK2 (**Fig. 8**, compare black bars vs. open and gray bars). An increase was observed in all the TG species monitored, suggesting no species specificity of the phenotype (Fig. 8 and supplementary Tables I, II). Furthermore, because mass spectrometry

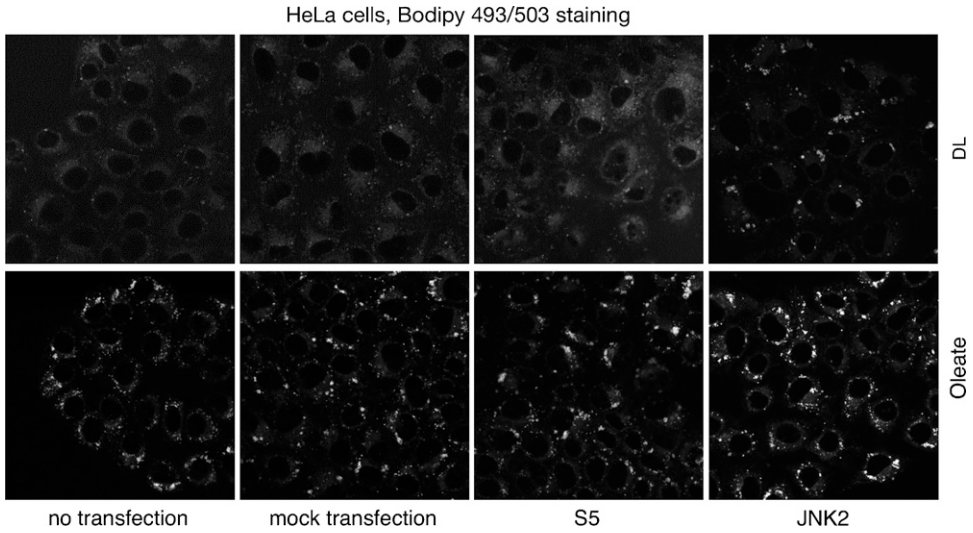

Fig. 7. Effect of JNK2 knock-down on the accumulation of lipid droplets. A431 cells were either untransfected, mock-transfected, or transfected with S5 or JNK2 siRNAs, as indicated. After 48 h, medium was replaced by a medium containing delipidated serum (DL) or a medium supplemented with oleate (oleate). Twenty-four hours later, cells were fixed, stained for neutral lipids with BODIPY 493/503, and imaged by confocal laser scanning microscopy.

does not require any labeling, these data demonstrate that the phenotype reflects the status of the entire TG pool of the cell and not only an increase in newly synthesized TG.

JNK2 is implicated in the regulation of lipolysis

An increase in TG can result either from an increase in lipid biosynthesis or import, or from a decrease in its degradation. Therefore, we used the general lipase inhibitor NBD-HEP (31) in combination with our knock-down assay. By blocking the lipase, NBD-HEP induced a strong increase in the TG level (**Fig. 9**, gray lines, +inhibitor). However, although in the absence of an inhibitor, the increase in TG was observed as seen previously in the JNK2 knock-down (Fig. 9, black vs. gray lines, no inhibitor), no difference was seen between the knock-down and the control after inhibitor treatment (Fig. 9, black vs. gray lines +inhibitor). This suggests that JNK2 affects lipase activity and has little or no effect on TG synthesis.

Sty1, a functional JNK2 homolog in *S. pombe*

To further confirm the specificity of the phenotype and the role of JNK2 in the regulation of TG metabolism, a JNK2 homolog in *S. pombe* was analyzed. Gene deletion in yeast is an established technique and it is therefore possible to study the effect of gene knock-out in that organism, a system much less prone to off-target effects. In contrast to human cells, *S. pombe* contains only one stress-activated MAPK, named Sty1 (32). Like JNK2, it is activated upon glucose deprivation (33, 34). Furthermore, complementation studies of the homolog of Sty1 in *Saccharomyces cerevisiae*, Hog1, showed that both mammalian JNK and p38 kinases, the two subfamilies of stress-activated MAPKs, could partially substitute for the loss of Hog1 (35, 36).

To investigate the regulatory function of Sty1 in TG metabolism, the accumulation of lipid droplets in the Sty1 deletion strain JM1160 was visualized. For this purpose, cells

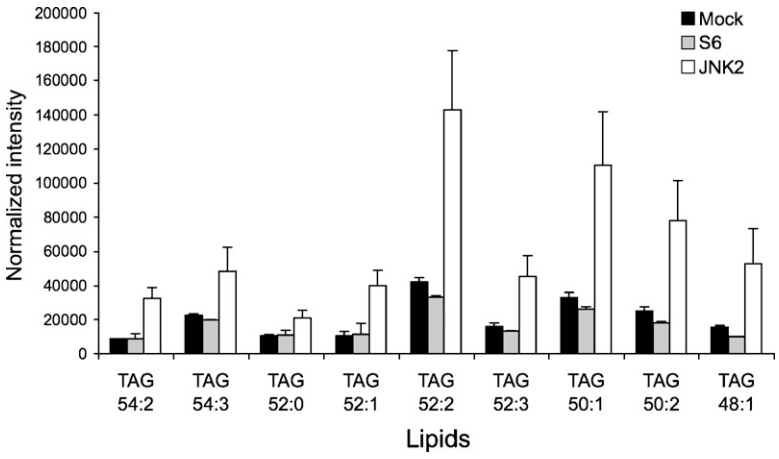

Fig. 8. Semi-quantitative MS of TG species. Individual sums of isobaric TG species were monitored by LTQ-Orbitrap MS for mock-transfected samples (black bars) or samples transfected with S6 (gray bars) or JNK2 (open bars) siRNAs. Values were normalized to the level of the most abundant lipid, PC 34:1, as described in Materials and Methods. The TG species are denoted, with two numbers being, respectively, the number of carbon atoms and the number of double bonds in the fatty acyl chains. Error bars represent the range of two experiments.

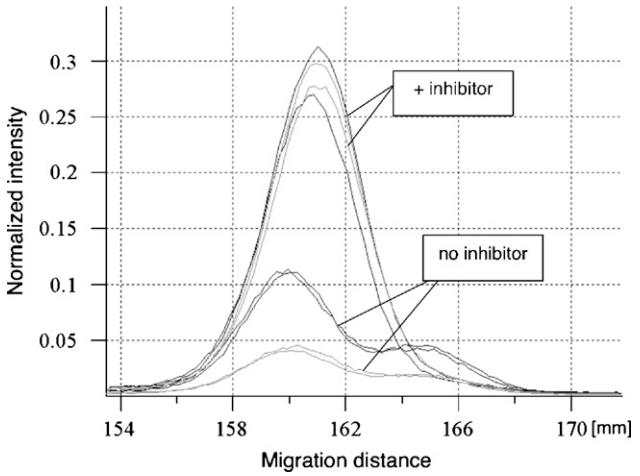

Fig. 9. Loss of JNK2 knock-down phenotype upon lipase inhibition. HeLa cells mock transfected (gray curves) or transfected with JNK2 siRNAs (Op, black curves) were treated with or without the lipase inhibitor NBD-D-HP as indicated. After ^{14}C labeling, lipids were separated on a TLC plate. A close-up of the storage lipid region from the lipid profiles obtained after TLC is shown. Intensities were normalized to the level of PC.

were labeled with the hydrophobic dye Nile Red, previously used in yeast to label lipid droplets (37, 38). As shown in **Fig. 10**, there is a strong increase in lipid droplet staining using Nile Red in the Sty1 deletion strain compared with the corresponding wild-type strain, suggesting a functional homology between the mammalian and the yeast protein.

DISCUSSION

Dysregulation of lipid metabolism is a major cause of some of the most common diseases in our societies. Understanding its molecular basis and identifying the players of this process are therefore major challenges for the identification of new potential drug targets. To this end, a screening procedure was developed that allows delineation of the implication of some genes in the maintenance of lipid homeostasis. This method is based on a combination of RNAi and lipid analysis by TLC, and has proven to be successful for observing alterations of lipid composition upon specific siRNA treatment. Using TLC as a read-out system, modifications can be observed in all lipid classes. However, most phenotypes affect cholesterol, CEs, and TGs. These lipids, more subject to variation in the human body upon changes in diet or health status, may be similarly more subject to variation in cells, whereas the pool of glycerophospholipids, probably because of their more structural role, is tightly regulated. In particular, several siRNAs induced a decrease in cholesterol and the appearance of an additional lipid band, presumably lanosterol or demethyllanosterol. This phenotype suggests that in addition to the known regulation of cholesterol biosynthesis at the level of HMG-CoA reductase (39), there is another major regulatory step at the level of these methylated sterols. Accordingly, it has recently been shown that lanosterol is instrumental in the downregulation of HMG-CoA reductase, promoting its regulation and degradation (40).

During our screen, a high proportion (15%) of kinase knock-downs gave rise to a phenotype. Although this number may seem high, other screens targeting kinases and phosphatases generated similar or even a higher number of hits (41, 42). Pelkmans et al. (42) showed that this high proportion of hits was intrinsic to the targeting of kinases, probably owing to their implication in a wide range of cellular processes. Interestingly, among the siRNAs affecting cholesterol metabolism that scored in our screen, siRNAs targeting IKK1, CSF1R, TRIO, and ATR were also shown to affect endocytosis in this previous screen, confirming the important role for cholesterol in this process.

However, the high number of phenotypes observed in the present screen could also result from a relatively high occurrence of off-target effects, as our results suggest. It was initially proposed that only genes showing a perfect complementarity to an siRNA would be targeted, and mismatches of just one nucleotide would be sufficient to disrupt this effect (13). However, more recently, several reports have suggested that this rule is not always applicable and that expression of several unintended genes is also affected upon the use of a given siRNA (26, 43–45). One possibility could be that siRNA molecules can be processed in the cells similarly to the endogenous microRNAs, inducing translational repression or even mRNA degradation of genes showing only partial complementarity to a given siRNA (46–48). Similar effects have also been reported in screens performed previously (43, 44). Several miRNAs have been implicated in the regulation of lipid metabolism (9–12). It is possible that several genes implicated in lipid homeostasis are targets of miRNAs and would therefore be more sensitive to unintended downregulation by siRNA (49, 50). However, improved siRNA design, which further restricts complementarity between siRNAs and unintended targets, should decrease the occurrence of off-target effects in later screens.

Despite the off-target problems encountered in the screen, we identified JNK2 as a new regulator of lipid droplet metabolism. Four independent siRNAs targeting JNK2 showed a consistent increase in TG upon RNAi.

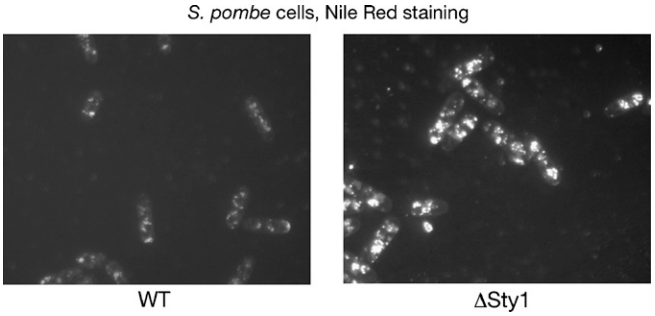

Fig. 10. Neutral lipid accumulation in *Schizosaccharomyces pombe* Sty1 deletion strain. The wild-type (WT) and the Sty1 deletion strains were stained with the neutral lipid dye Nile Red and imaged in a wide-field fluorescent microscope.

The increase in TG could be confirmed by both TLC and mass spectrometry. Furthermore, a similar phenotype was observed using an inhibitor of JNK. This effect was also coupled to an increase in lipid droplets, as observed by BODIPY 493/503 staining upon JNK2 knock-down.

To further confirm the specificity of the phenotype, a homolog of JNK2 in *S. pombe*, Sty1, was also analyzed. Deletion of this gene induced both an increase in TG and an increase in lipid droplets. Together, these data suggest that both JNK2 and its *S. pombe* homolog, Sty1, are implicated in the regulation of TG and lipid droplet metabolism.

It should be noted that in another study (51), treatment with siRNA against JNK2 did not result in a phenotype of increased lipid droplets. However, this study was performed with a single siRNA sequence only, using oleate feeding conditions instead of low-lipid conditions, and in a different cell line (NIH-3T3), each of which can explain the difference in our findings.

Previous works with knock-out mice have shown an implication of JNK2 in two lipid-related pathologies, obesity and atherosclerosis (52, 53). Total JNK activity is enhanced by obesity (54). This appeared to be mostly due to JNK1, because it was not observed in highly fed JNK1 knock-out mice. Moreover, JNK1 knock-out mice were resistant to obesity, whereas JNK2 knock-out mice did not show any obesity-related phenotype (54). However, crossing these mice, Tuncman et al. (52) showed that the offspring with the phenotype $JNK1^{+/-}$ $JNK2^{-/-}$ were also resistant to obesity, suggesting that the implication of JNK2 in fat accumulation was masked by JNK1 activity in the single knock-out. Another major disease that can arise from dysregulation of lipid metabolism is atherosclerosis. Activation of JNK2 was observed in atherosclerotic lesions, in both mice and humans (53, 55). Deletion of JNK2, but not JNK1, in an atherosclerosis mouse model decreased the occurrence of the lesions (53). This appeared to be the result of a decrease in LDL internalization by macrophages, following defective phosphorylation of scavenger receptor A, one of the main receptors for modified LDL, and a concomitant decrease in foam cell formation (53). However, because in our assay the phenotype is also observed in delipidated conditions, JNK2 must also influence TG metabolism directly at the intracellular level, either via inhibition of TG synthesis or by promoting its degradation. JNK proteins and their *S. pombe* homolog, Sty1, are activated upon glucose depletion (33, 34). Under these conditions, cells need to obtain their energy from other sources, such as TG. Interestingly, upon activation of Sty1, several genes involved in peroxisomal β oxidation are upregulated (56), suggesting the implication of the kinase in energy metabolism. Our data show that upon inhibition of lipase activity, no further increase in TG could be observed in the knock-down of JNK2. We can therefore conclude that the kinase does not influence the biosynthesis of TG, but rather its degradation via modulation of lipase activity. In adipocytes, TNFα has been shown to induce lipolysis in a JNK-dependent fashion (57) via downregulation of perilipin expression, a lipid droplet-associated protein thought to modulate the access of the lipases to the lipid droplet surface (58). Perilipin is not expressed in nonadipose tissues, but a similar mechanism could take place with a yet-unidentified lipid droplet protein.

Further analysis of the implication of JNK2 in lipid droplet metabolism will be required to fully understand its implication in TG lipolysis. Nevertheless, JNK2 appears to be an interesting drug target, not only for the treatment of atherosclerosis (59–61), but also in the treatment of other lipid-related diseases.

The authors would like to thank J. B. Millar (University of Warwick, UK) for providing the *S. pombe* deletion strain.

REFERENCES

1. Murray, C. J., and A. D. Lopez. 1997. Global mortality, disability, and the contribution of risk factors: Global Burden of Disease Study. *Lancet.* **349:** 1436–1442.
2. Caballero, B. 2005. A nutrition paradox—underweight and obesity in developing countries. *N. Engl. J. Med.* **352:** 1514–1516.
3. Rawson, R. B. 2003. The SREBP pathway—insights from Insigs and insects. *Nat. Rev. Mol. Cell Biol.* **4:** 631–640.
4. Beaven, S. W., and P. Tontonoz. 2006. Nuclear receptors in lipid metabolism: targeting the heart of dyslipidemia. *Annu. Rev. Med.* **57:** 313–329.
5. Zelcer, N., and P. Tontonoz. 2006. Liver X receptors as integrators of metabolic and inflammatory signaling. *J. Clin. Invest.* **116:** 607–614.
6. Kalaany, N. Y., and D. J. Mangelsdorf. 2006. LXRS and FXR: the yin and yang of cholesterol and fat metabolism. *Annu. Rev. Physiol.* **68:** 159–191.
7. Li, A. C., and C. K. Glass. 2004. PPAR- and LXR-dependent pathways controlling lipid metabolism and the development of atherosclerosis. *J. Lipid Res.* **45:** 2161–2173.
8. Chawla, A., J. J. Repa, R. M. Evans, and D. J. Mangelsdorf. 2001. Nuclear receptors and lipid physiology: opening the X-files. *Science.* **294:** 1866–1870.
9. Krutzfeldt, J., N. Rajewsky, R. Braich, K. G. Rajeev, T. Tuschl, M. Manoharan, and M. Stoffel. 2005. Silencing of microRNAs in vivo with 'antagomirs'. *Nature.* **438:** 685–689.
10. Krutzfeldt, J., and M. Stoffel. 2006. MicroRNAs: a new class of regulatory genes affecting metabolism. *Cell Metab.* **4:** 9–12.
11. Xu, P., S. Y. Vernooy, M. Guo, and B. A. Hay. 2003. The Drosophila microRNA Mir-14 suppresses cell death and is required for normal fat metabolism. *Curr. Biol.* **13:** 790–795.
12. Esau, C., S. Davis, S. F. Murray, X. X. Yu, S. K. Pandey, M. Pear, L. Watts, S. L. Booten, M. Graham, R. McKay, et al. 2006. miR-122 regulation of lipid metabolism revealed by in vivo antisense targeting. *Cell Metab.* **3:** 87–98.
13. Elbashir, S. M., J. Harborth, W. Lendeckel, A. Yalcin, K. Weber, and T. Tuschl. 2001. Duplexes of 21-nucleotide RNAs mediate RNA interference in cultured mammalian cells. *Nature.* **411:** 494–498.
14. Fire, A., S. Xu, M. K. Montgomery, S. A. Kostas, S. E. Driver, and C. C. Mello. 1998. Potent and specific genetic interference by double-stranded RNA in Caenorhabditis elegans. *Nature.* **391:** 806–811.
15. Carpenter, A. E., and D. M. Sabatini. 2004. Systematic genome-wide screens of gene function. *Nat. Rev. Genet.* **5:** 11–22.
16. Dorsett, Y., and T. Tuschl. 2004. siRNAs: applications in functional genomics and potential as therapeutics. *Nat. Rev. Drug Discov.* **3:** 318–329.
17. Thiele, C., M. J. Hannah, F. Fahrenholz, and W. B. Huttner. 2000. Cholesterol binds to synaptophysin and is required for biogenesis of synaptic vesicles. *Nat. Cell Biol.* **2:** 42–49.
18. Kuerschner, L., C. S. Ejsing, K. Ekroos, A. Shevchenko, K. I. Anderson, and C. Thiele. 2005. Polyene-lipids: a new tool to image lipids. *Nat. Methods.* **2:** 39–45.
19. Kalaidzidis, Y. L., A. V. Gavrilov, P. V. Zaitsev, A. L. Kalaidzidis, and E. V. Korolev. 1997. PLUK—an environment for software development. *Program. Comput. Softw.* **23:** 206–212.

20. Forsburg, S. L., and N. Rhind. 2006. Basic methods for fission yeast. *Yeast.* **23:** 173–183.
21. Harborth, J., S. M. Elbashir, K. Bechert, T. Tuschl, and K. Weber. 2001. Identification of essential genes in cultured mammalian cells using small interfering RNAs. *J. Cell Sci.* **114:** 4557–4565.
22. Weil, D., L. Garcon, M. Harper, D. Dumenil, F. Dautry, and M. Kress. 2002. Targeting the kinesin Eg5 to monitor siRNA transfection in mammalian cells. *Biotechniques.* **33:** 1244–1248.
23. Harborth, J., S. M. Elbashir, K. Vandenburgh, H. Manninga, S. A. Scaringe, K. Weber, and T. Tuschl. 2003. Sequence, chemical, and structural variation of small interfering RNAs and short hairpin RNAs and the effect on mammalian gene silencing. *Antisense Nucleic Acid Drug Dev.* **13:** 83–105.
24. Holen, T., M. Amarzguioui, M. T. Wiiger, E. Babaie, and H. Prydz. 2002. Positional effects of short interfering RNAs targeting the human coagulation trigger Tissue Factor. *Nucleic Acids Res.* **30:** 1757–1766.
25. Kwok, B. H., B. Koh, M. I. Ndubuisi, M. Elofsson, and C. M. Crews. 2001. The anti-inflammatory natural product parthenolide from the medicinal herb Feverfew directly binds to and inhibits IkappaB kinase. *Chem. Biol.* **8:** 759–766.
26. Jackson, A. L., S. R. Bartz, J. Schelter, S. V. Kobayashi, J. Burchard, M. Mao, B. Li, G. Cavet, and P. S. Linsley. 2003. Expression profiling reveals off-target gene regulation by RNAi. *Nat. Biotechnol.* **21:** 635–637.
27. Bennett, B. L., D. T. Sasaki, B. W. Murray, E. C. O'Leary, S. T. Sakata, W. Xu, J. C. Leisten, A. Motiwala, S. Pierce, Y. Satoh, et al. 2001. SP600125, an anthrapyrazolone inhibitor of Jun N-terminal kinase. *Proc. Natl. Acad. Sci. USA.* **98:** 13681–13686.
28. Brown, D. A. 2001. Lipid droplets: proteins floating on a pool of fat. *Curr. Biol.* **11:** R446–R449.
29. Gocze, P. M., and D. A. Freeman. 1994. Factors underlying the variability of lipid droplet fluorescence in MA-10 Leydig tumor cells. *Cytometry.* **17:** 151–158.
30. Schwudke, D., J. T. Hannich, V. Surendranath, V. Grimard, T. Moehring, L. Burton, T. Kurzchalia, and A. Shevchenko. 2007. Top-down lipidomic screens by multivariate analysis of high-resolution survey mass spectra. *Anal. Chem.* **79:** 4083–4093.
31. Oskolkova, O. V., R. Saf, E. Zenzmaier, and A. Hermetter. 2003. Fluorescent organophosphonates as inhibitors of microbial lipases. *Chem. Phys. Lipids.* **125:** 103–114.
32. Degols, G., K. Shiozaki, and P. Russell. 1996. Activation and regulation of the Spc1 stress-activated protein kinase in Schizosaccharomyces pombe. *Mol. Cell. Biol.* **16:** 2870–2877.
33. Stettler, S., E. Warbrick, S. Prochnik, S. Mackie, and P. Fantes. 1996. The wis1 signal transduction pathway is required for expression of cAMP-repressed genes in fission yeast. *J. Cell Sci.* **109:** 1927–1935.
34. Liu, X., A. K. Gupta, P. M. Corry, and Y. J. Lee. 1997. Hypoglycemia-induced c-Jun phosphorylation is mediated by c-Jun N-terminal kinase 1 and Lyn kinase in drug-resistant human breast carcinoma MCF-7/ADR cells. *J. Biol. Chem.* **272:** 11690–11693.
35. Galcheva-Gargova, Z., B. Derijard, I. H. Wu, and R. J. Davis. 1994. An osmosensing signal transduction pathway in mammalian cells. *Science.* **265:** 806–808.
36. Han, J., J. D. Lee, L. Bibbs, and R. J. Ulevitch. 1994. A MAP kinase targeted by endotoxin and hyperosmolarity in mammalian cells. *Science.* **265:** 808–811.
37. Greenspan, P., E. P. Mayer, and S. D. Fowler. 1985. Nile red: a selective fluorescent stain for intracellular lipid droplets. *J. Cell Biol.* **100:** 965–973.
38. Tong, F., P. N. Black, L. Bivins, S. Quackenbush, V. Ctrnacta, and C. C. DiRusso. 2006. Direct interaction of Saccharomyces cerevisiae Faa1p with the Omi/HtrA protease orthologue Ynm3p alters lipid homeostasis. *Mol. Genet. Genomics.* **275:** 330–343.
39. Goldstein, J. L., and M. S. Brown. 1990. Regulation of the mevalonate pathway. *Nature.* **343:** 425–430.
40. Song, B. L., N. B. Javitt, and R. A. DeBose-Boyd. 2005. Insig-mediated degradation of HMG CoA reductase stimulated by lanosterol, an intermediate in the synthesis of cholesterol. *Cell Metab.* **1:** 179–189.
41. MacKeigan, J. P., L. O. Murphy, and J. Blenis. 2005. Sensitized RNAi screen of human kinases and phosphatases identifies new regulators of apoptosis and chemoresistance. *Nat. Cell Biol.* **7:** 591–600.
42. Pelkmans, L., E. Fava, H. Grabner, M. Hannus, B. Habermann, E. Krausz, and M. Zerial. 2005. Genome-wide analysis of human kinases in clathrin- and caveolae/raft-mediated endocytosis. *Nature.* **436:** 78–86.
43. Lin, X., X. Ruan, M. G. Anderson, J. A. McDowell, P. E. Kroeger, S. W. Fesik, and Y. Shen. 2005. siRNA-mediated off-target gene silencing triggered by a 7 nt complementation. *Nucleic Acids Res.* **33:** 4527–4535.
44. Ma, Y., A. Creanga, L. Lum, and P. A. Beachy. 2006. Prevalence of off-target effects in Drosophila RNA interference screens. *Nature.* **443:** 359–363.
45. Birmingham, A., E. M. Anderson, A. Reynolds, D. Ilsley-Tyree, D. Leake, Y. Fedorov, S. Baskerville, E. Maksimova, K. Robinson, J. Karpilow, et al. 2006. 3′ UTR seed matches, but not overall identity, are associated with RNAi off-targets. *Nat. Methods.* **3:** 199–204.
46. Doench, J. G., C. P. Petersen, and P. A. Sharp. 2003. siRNAs can function as miRNAs. *Genes Dev.* **17:** 438–442.
47. Lim, L. P., N. C. Lau, P. Garrett-Engele, A. Grimson, J. M. Schelter, J. Castle, D. P. Bartel, P. S. Linsley, and J. M. Johnson. 2005. Microarray analysis shows that some microRNAs downregulate large numbers of target mRNAs. *Nature.* **433:** 769–773.
48. Zeng, Y., R. Yi, and B. R. Cullen. 2003. MicroRNAs and small interfering RNAs can inhibit mRNA expression by similar mechanisms. *Proc. Natl. Acad. Sci. USA.* **100:** 9779–9784.
49. Stark, A., J. Brennecke, N. Bushati, R. B. Russell, and S. M. Cohen. 2005. Animal microRNAs confer robustness to gene expression and have a significant impact on 3′UTR evolution. *Cell.* **123:** 1133–1146.
50. Jackson, A. L., J. Burchard, J. Schelter, B. N. Chau, M. Cleary, L. Lim, and P. S. Linsley. 2006. Widespread siRNA "off-target" transcript silencing mediated by seed region sequence complementarity. *RNA.* **12:** 1179–1187.
51. Andersson, L., P. Bostrom, J. Ericson, M. Rutberg, B. Magnusson, D. Marchesan, M. Ruiz, L. Asp, P. Huang, M. A. Frohman, et al. 2006. PLD1 and ERK2 regulate cytosolic lipid droplet formation. *J. Cell Sci.* **119:** 2246–2257.
52. Tuncman, G., J. Hirosumi, G. Solinas, L. Chang, M. Karin, and G. S. Hotamisligil. 2006. Functional in vivo interactions between JNK1 and JNK2 isoforms in obesity and insulin resistance. *Proc. Natl. Acad. Sci. USA.* **103:** 10741–10746.
53. Ricci, R., G. Sumara, I. Sumara, I. Rozenberg, M. Kurrer, A. Akhmedov, M. Hersberger, U. Eriksson, F. R. Eberli, B. Becher, et al. 2004. Requirement of JNK2 for scavenger receptor A-mediated foam cell formation in atherogenesis. *Science.* **306:** 1558–1561.
54. Hirosumi, J., G. Tuncman, L. Chang, C. Z. Gorgun, K. T. Uysal, K. Maeda, M. Karin, and G. S. Hotamisligil. 2002. A central role for JNK in obesity and insulin resistance. *Nature.* **420:** 333–336.
55. Nishio, H., K. Matsui, H. Tsuji, A. Tamura, and K. Suzuki. 2001. Immunohistochemical study of the phosphorylated and activated form of c-Jun NH2-terminal kinase in human aorta. *Histochem. J.* **33:** 167–171.
56. Chen, D., W. M. Toone, J. Mata, R. Lyne, G. Burns, K. Kivinen, A. Brazma, N. Jones, and J. Bahler. 2003. Global transcriptional responses of fission yeast to environmental stress. *Mol. Biol. Cell.* **14:** 214–229.
57. Ryden, M., E. Arvidsson, L. Blomqvist, L. Perbeck, A. Dicker, and P. Arner. 2004. Targets for TNF-alpha-induced lipolysis in human adipocytes. *Biochem. Biophys. Res. Commun.* **318:** 168–175.
58. Souza, S. C., L. M. de Vargas, M. T. Yamamoto, P. Lien, M. D. Franciosa, L. G. Moss, and A. S. Greenberg. 1998. Overexpression of perilipin A and B blocks the ability of tumor necrosis factor alpha to increase lipolysis in 3T3-L1 adipocytes. *J. Biol. Chem.* **273:** 24665–24669.
59. Manning, A. M., and R. J. Davis. 2003. Targeting JNK for therapeutic benefit: from junk to gold? *Nat. Rev. Drug Discov.* **2:** 554–565.
60. Karin, M., and E. Gallagher. 2005. From JNK to pay dirt: jun kinases, their biochemistry, physiology and clinical importance. *IUBMB Life.* **57:** 283–295.
61. Sumara, G., M. Belwal, and R. Ricci. 2005. "Jnking" atherosclerosis. *Cell. Mol. Life Sci.* **62:** 2487–2494.